ACS APPLIED MATERIALS & INTERFACES

www.acsami.org

Research Article

Linker Engineering of 2D Imine Covalent Organic Frameworks for the Heterogeneous Palladium-Catalyzed Suzuki Coupling Reaction

Chidharth Krishnaraj,*[,‖] Himanshu Sekhar Jena,[‖] Kuber Singh Rawat, Johannes Schmidt, Karen Leus, Veronique Van Speybroeck, and Pascal Van Der Voort*

Cite This: *ACS Appl. Mater. Interfaces* 2022, 14, 50923−50931

Read Online

ACCESS | Metrics & More | Article Recommendations | Supporting Information

ABSTRACT: Covalent organic frameworks (COFs) are an emerging class of porous organic polymers that have been utilized as scaffolds for anchoring metal active species to act as heterogeneous catalysts. Though several examples of such COFs exist, a thorough experimental and computational analysis on such catalysts is limited. In this work, a series of two-dimensional (2D) imine COFs (TTA−DFB COF (N), TTA−TBD COF (N∧O), and TTA−DFP COF(N∧N)) were synthesized by using suitable building units to obtain three different coordination sites (N, N∧O, and N∧N). These were post-modified with Pd(II) to catalyze the Suzuki−Miyaura coupling reaction. Pd@TTA−DFB COF, where Pd(II) was coordinated to N sites, showed the fastest reactivity and lower stability. Pd@TTA−DFP COF showed highest stability but slowest reactivity. Pd@TTA−TBD COF was the best among the three with both high stability and fast reactivity. By combining both experimental and computational results, we conclude that the Pd(II) to Pd(0) reduction is a key step in the difference between the catalytic reactivities of the three COFs. This study demonstrates the importance of the building block approach to design COFs for efficient heterogeneous catalysis and to understand the fate of the reaction profile.

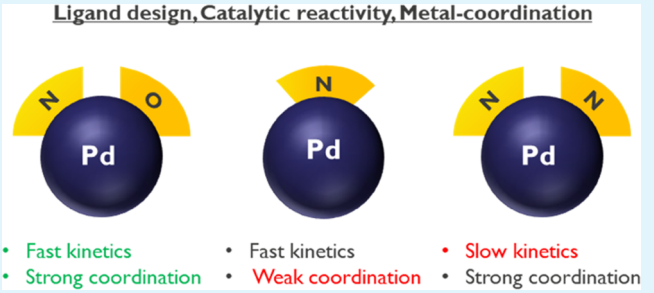

KEYWORDS: *covalent organic frameworks, Suzuki coupling reaction, palladium catalysis, linker modification, reticular synthesis*

INTRODUCTION

Covalent organic frameworks (COFs) have gained attention in recent years owing to their mild synthesis, high molecular-level ordering, tunable structure and properties, and diverse field of applications.[1] Rigid building blocks are bonded together through strong covalent linkages to result in rigid porous structures. An important aspect in the formation of a crystalline COF is to utilize the reversible nature of covalent chemical reactions.[2] Several reversible covalent linkages have been explored for synthesizing COFs. However, COFs produced using imine condensation reactions have become widely popular due to the wide scope of linkers and mild synthesis conditions.

COFs have been explored for various applications such as waste-water treatment,[3,4] gas adsorption and storage,[5,6] optoelectronics,[7] and catalysis.[8] Particularly in catalysis, both metal-free[9,10] and metal-based heterogeneous catalysts[11−14] have been studied. Catalysis has been performed with the aid of active metal catalysts anchored to two nitrogen atoms present on two stacked two-dimensional (2D) COF sheets.[15] Other reports also include metal immobilization due to physiosorption[16] and partial stabilization in the presence of mono-nitrogen atoms[17] and defect sites.[18] Though these results depict good catalytic activity, there can be problems of metal leaching due to the mechanical stress causing destruction or delamination of the COFs during the catalytic reaction (stirring and refluxing). Additionally, usage of bipyridine,[19] porphyrinic,[20] or NHC-type[21] metal anchoring sites incorporated in the COF structure has resulted in efficient metal complexation.

Alternatively, the reticular principles[22] of COF construction can be exploited to easily engineer various metal anchoring sites on the COFs, based on contemplative selection of the starting linkers. Reticular principles allow prediction and tunability of the COF geometry by variation in the type and symmetry of molecular building blocks. Synthesis and purification of imine COFs have become easier to do under ambient conditions.[23] Hence, we chose COF as a perfect platform to study the effects of linker engineering. In this study, we report three isoreticular 2D imine COFs, namely TTA−DFB COF, TTA−TBD COF, and TTA−DFP COF,[24] which have a common tri-topic linker and a carefully selected second di-topic linker providing functional variation. The

Received: August 18, 2022
Accepted: October 24, 2022
Published: November 7, 2022

Scheme 1. Formation of TTA−DFB COF (N), TTA−TBD COF (N∧O), and TTA−DFP COF (N∧N)

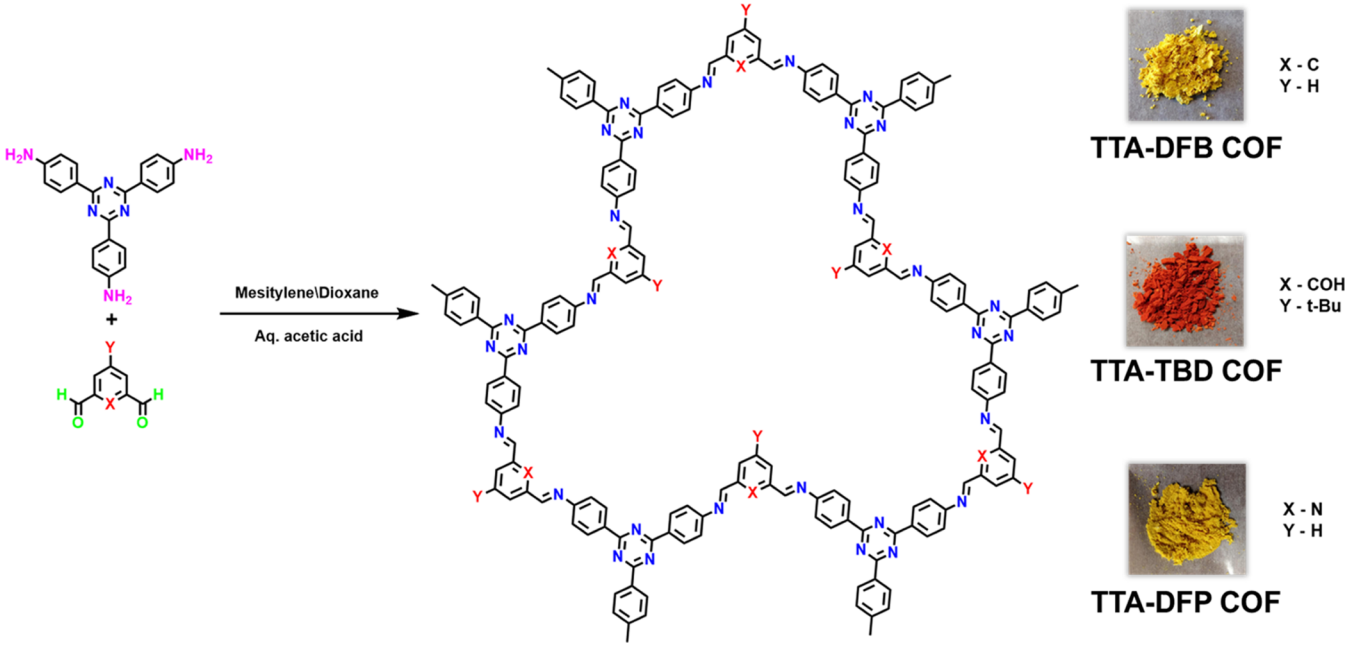

imine nitrogen along with the varying functionalities in the ditopic linkers creates three different coordination pockets for metal coordination. Using this simple strategy of linker engineering allowed us to design three different types of metal anchoring sites containing N-, N∧O-, and N∧N-rich regions on TTA−DFB COF, TTA−TBD COF, and TTA−DFP COF, respectively.

The well-known palladium-catalyzed Suzuki−Miyaura coupling[25] is used as a study model to explore the variation in reactivity and mechanisms of the three different types of ancillary ligands on the COFs. Suzuki−Miyaura cross-coupling reactions are considered as one of the most important cross-coupling reactions in the pharmaceutical, fine chemical, and electronic industries.[26,27] Palladium-assisted Suzuki−Miyaura cross-coupling has been explored in-depth previously.[28] Especially, the stereo-electronic properties and coordination nature of homogeneous ligands such as NHC and phosphine in Suzuki−Miyaura cross-coupling have been well studied.[28,29] However, in industries, heterogeneous catalysts are preferred since they provide advantages such as reusability, easy recovery and regeneration, higher turnover numbers, and sustainable usage over homogeneous catalysts. Several heterogeneous catalysts such as PMOs,[30] metal−organic frameworks (MOFs),[31] activated carbon,[32] and COFs[33] that act as support for palladium have been reported. The factors concerning their stereo-electronic properties depend on the COF structure.[34] Linker engineering was utilized in bipyridyl-MOFs to synthesize an efficient support for Pd(II)-based Suzuki coupling reactions.[35] This served as a great approach to design efficient catalysts. To overcome metal leaching issues, a strong coordination site on the COFs is required. Herein, aiming at efficient selection of anchoring sites for metal-based catalysis, we report a comparative study on three different types of ancillary ligands engineered on COFs and their corresponding impact on the catalytic activity in palladium-based Suzuki−Miyaura coupling reactions.

RESULTS AND DISCUSSION

Three different batches of TTA-mesitylene/dioxane solutions were prepared and mixed with (A) DFB-mesitylene-dioxane solution, (B) TBD-mesitylene-dioxane solution, and (C) DFP-mesitylene-dioxane solution to produce three isoreticular COFs, namely (1) TTA−DFB COF (N), (2) TTA−TBD COF (N∧O), and (3) TTA−DFP COF (N∧N), respectively (Scheme 1). TTA−TBD (N∧O) and TTA−DFB (N) COFs are novel COFs, whereas TTA−DFP (N∧N) COF has been reported in our previous work.[24] Aqueous acetic acid was added to the solutions to accelerate the imine-condensation-based polymerization process. The synthesized COFs are insoluble in water or common organic solvents (such as tetrahydrofuran, diethyl ether, acetone, methanol, ethanol, *N*,*N*-dimethylformamide, dichloromethane, trichloromethane, dimethyl sulfoxide).

The formation of the imine bond (−C═N) was confirmed by the presence of a stretch at 1680−1690 cm^{-1} in the Fourier transform infrared (FT-IR) spectra (Figure 1(i)). In comparison to the FT-IR spectrum of the TTA monomer and the corresponding aldehyde monomers, the peaks of aldehyde (1710 cm^{-1}) and amines (3300−3400cm^{-1}) in the COFs are greatly attenuated (Figure S1), which further implies the successful imine condensation. However, due to the unreacted aldehydes and amines at the terminal edges of the COF, residual signals were seen, which have been previously reported in such imine COFs.[33] In the case of TTA−TBD (N∧O) COF, a strong peak at 2965 cm^{-1} corresponding to the presence of the *t*-butyl group was observed, confirming the structural unit preservation during the polymerization process. Elemental analysis was used to calculate the amounts of C, H, N, and O in the COFs. Table S1 shows the relevant elemental content of the three COFs and their corresponding theoretical values. The experimental C/N ratio is close to the theoretical values, further providing evidence for the successful formation of the expected imine-linked COFs. Powder X-ray diffraction (PXRD) analysis was used to determine the crystalline structure of the synthesized COFs. Figure 1(ii) shows the

https://doi.org/10.1021/acsami.2c14882
ACS Appl. Mater. Interfaces 2022, 14, 50923−50931

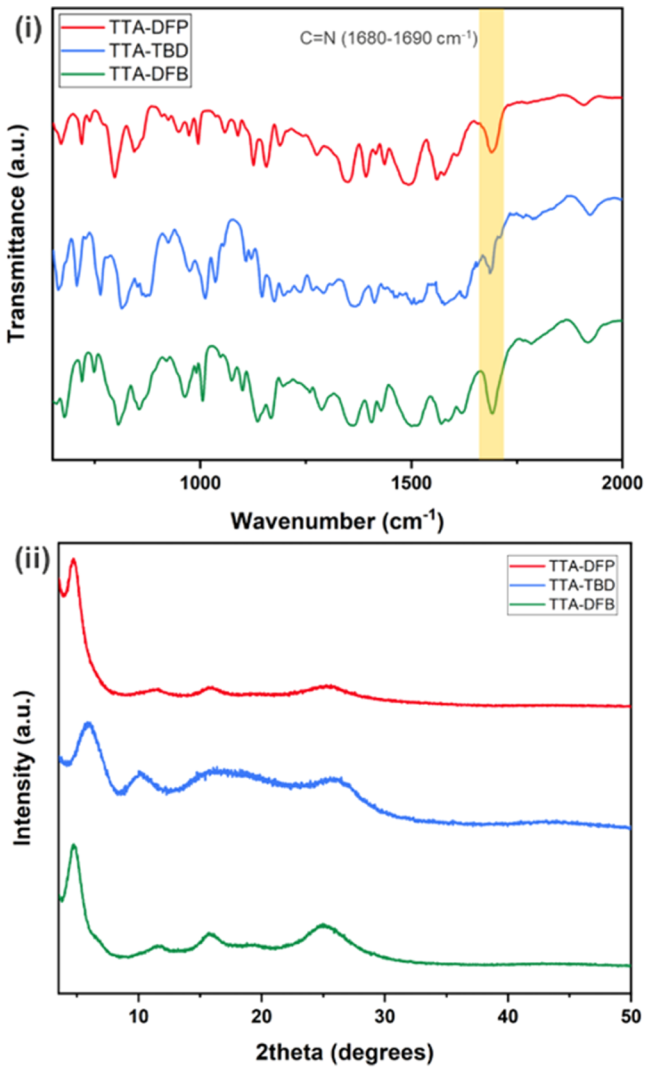

Figure 1. (i) FT-IR spectra and (ii) PXRD patterns of TTA−DFB (N), TTA−TBD (N∧O), and TTA−DFP (N∧N) COFs.

PXRD patterns of the COFs indicating a crystalline framework formation. The PXRD pattern of TTA−DFP (N∧N) matches well with the previous reports.[24] The PXRD pattern of TTA−DFB and TTA−TBD exhibited intense reflections in the low-angle region at 5.4° 2θ (d spacing ∼ 1.6 nm). The PXRD patterns displayed broad diffraction peaks at ∼26° 2θ indicating the formation of 2D layered material stacking in the c direction. The COF models were geometrically optimized and their simulated PXRD patterns matched the experimental patterns (Figure S2). The diffraction patterns of the starting monomers (Figure S3) are not visible in the diffraction patterns of the COFs, indicating the transformation of the starting monomers. The synthesized COFs are indeed not completely crystalline as the PXRD patterns are relatively broad.

Figure 2 shows the ^{13}C CP/MAS NMR spectra of the COFs. The ^{13}C NMR peak at 156−157 ppm corresponds to the characteristic imine carbon atom of the C═N bond. The signals at other regions are assigned to the carbon atoms of the phenyl and triazine groups. The minor peaks at 110−111 and 186−187 ppm are due to the unreacted terminal monomers in the COF framework. Additionally, in TTA−TBD (N∧O) COF, peaks at 30.5 and 27.5 ppm appear, confirming the presence of the t-butyl group in the structure.

Nitrogen (N_2) adsorption−desorption isotherms were measured at 77 K to characterize the porous properties of the COFs. Figure 3 shows a sharp increase in the gas uptake observed at low relative pressure (P/P_0 < 0.1) for all of the three COFs. They produce a Type-1 adsorption isotherm showing the microporous nature of the materials. The rise in the isotherms at higher relative pressures (0.8−0.99 P/P_0) corresponds to the presence of textural mesopores due to agglomeration of the COF crystals.[36] The Brunauer−Emmett−Teller (BET) surface areas are 30, 293, and 314 m^2/g and Langmuir surface areas are 50, 382, and 412 m^2/g for TTA−DFB (N), TTA−TBD (N∧O), and TTA−DFP (N∧N) COFs, respectively. The ideal porosity of a modelled fully crystalline COF could not be compared here because the synthesis only leads to partially crystalline COFs as seen from the PXRD patterns. Even after several attempts, the surface area of the COFs could not be improved further. The list of conditions attempted for the COF synthesis is provided in Table S2. Especially for TTA−DFB COF, it is possible that it gets

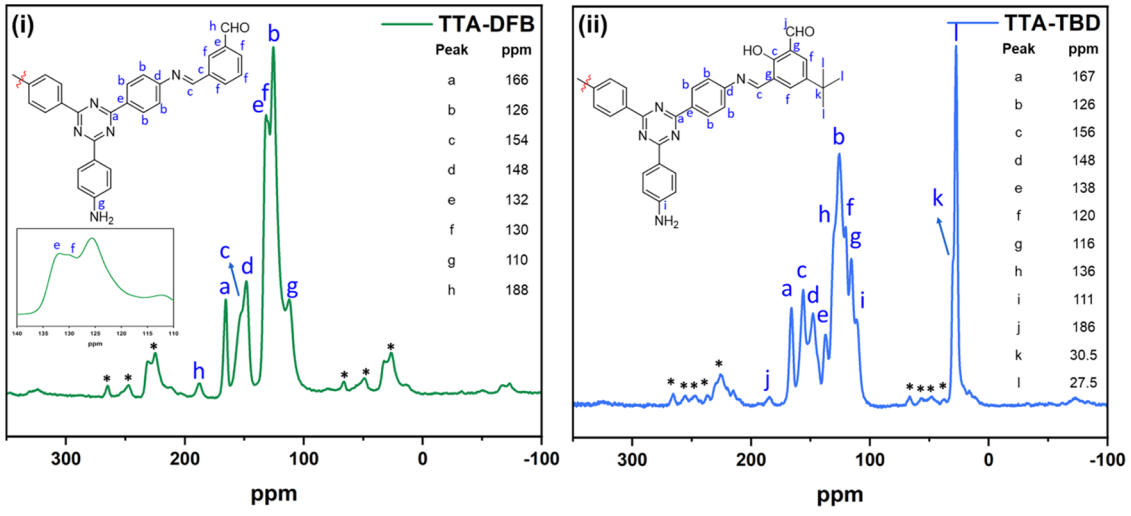

Figure 2. ^{13}C CP/MAS NMR spectra of (i) TTA−DFB (N) and (ii) TTA−TBD (N∧O) COFs with the corresponding peak assignments.

https://doi.org/10.1021/acsami.2c14882
ACS Appl. Mater. Interfaces 2022, 14, 50923−50931

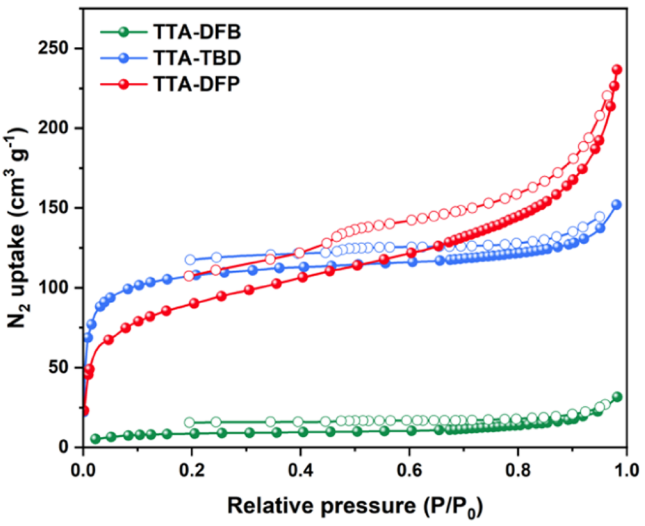

Figure 3. Nitrogen adsorption/desorption isotherms of the three COFs.

exfoliated and becomes COF nanosheets. Such behavior has been reported in the literature.[37−41]

Ligands containing N, N∧O, and N∧N functional groups are well known to coordinate metal complexes and have been widely studied concerning homogeneous catalysis.[42] Linker engineering of COFs has provided an easy platform to create stable porous materials along with the specific ancillary ligand coordination sites (N, N∧O, and N∧N) required to support metal complexes. In this study, Pd@COF catalysts were synthesized by postsynthetic metalation of the COFs with $Pd(OAc)_2$ in tetrahydrofuran. Equal amounts of palladium acetate were added to the three COFs to maintain uniform metalation conditions to compare the metal loading capacities of the three anchoring sites. Figure 4 shows an ideal representation of $Pd(OAc)_2$ anchoring on the ancillary ligands of the three COFs. PXRD patterns of the metalated COFs show that the crystallinity is retained after postsynthetic metalation (Figure S4). The order of the metal loading capacities of the three COFs is Pd@TTA−DFP (N∧N) > Pd@TTA−DFB (N) > Pd@TTA−TBD (N∧O).

For all of the metalated COFs, the N_2 adsorption−desorption isotherms show a decrease in the overall nitrogen uptake in all cases as expected. The Langmuir surface areas decreased to 20 m^2/g for Pd@TTA−DFB (N), 60 m^2/g for Pd@TTA−DFP (N∧N), and 324 m^2/g for Pd@TTA−TBD (N∧O) (Figure S5). X-ray photoelectron spectroscopy (XPS) measurements on Pd@TTA−DFB (N), Pd@TTA−TBD (N∧O), and Pd@TTA−DFP (N∧N) COFs (Figures S6−S8) revealed the binding energy (BE) of $Pd3d_{5/2}$ at 337.5 eV, corresponding to the +2 oxidation state.[43] Imine groups donate electrons to Pd(II), making it less electron-deficient. From the XPS analysis it is observed that in all cases, most of the palladium species remain with +2 oxidation states after loading onto the COFs. Also, palladium nanoparticles (Pd(0)) are observed in the materials, which could be due to partial reduction occurring during the measurements. In addition, the FT-IR spectra of the metalated COFs remained similar to the pure COF spectra (Figure S9).

To assess the impact of linker engineering in catalytic application, the palladium-catalyzed Suzuki−Miyaura cross-coupling reaction was chosen, where aryl halide reacts with aryl boronic acid to give bi-aryl as a product in the presence of Pd@COF as the catalyst. The reaction mechanism for the formation of C−C bonds under homogeneous conditions has been widely studied and is shown in Scheme S1. The standard Suzuki−Miyaura cross-coupling mechanism involves three important steps: (i) oxidative addition, where aryl bromide (R_1-Br) attaches to palladium, and subsequently, bromine is replaced by OCO^{2-} ion from the base; (ii) transmetalation, where the OCO^{2-} ion is replaced by the aryl (R_2) group; and (iii) reductive elimination, where R_1-R_2 is eliminated, reverting the palladium back to its original form. In case of the three COFs in our study, monodentate (TTA−DFB with N) and bidentate (TTA−TBD with N∧O and TTA−DFP with N∧N) ligands are present. Due to this varying chelating

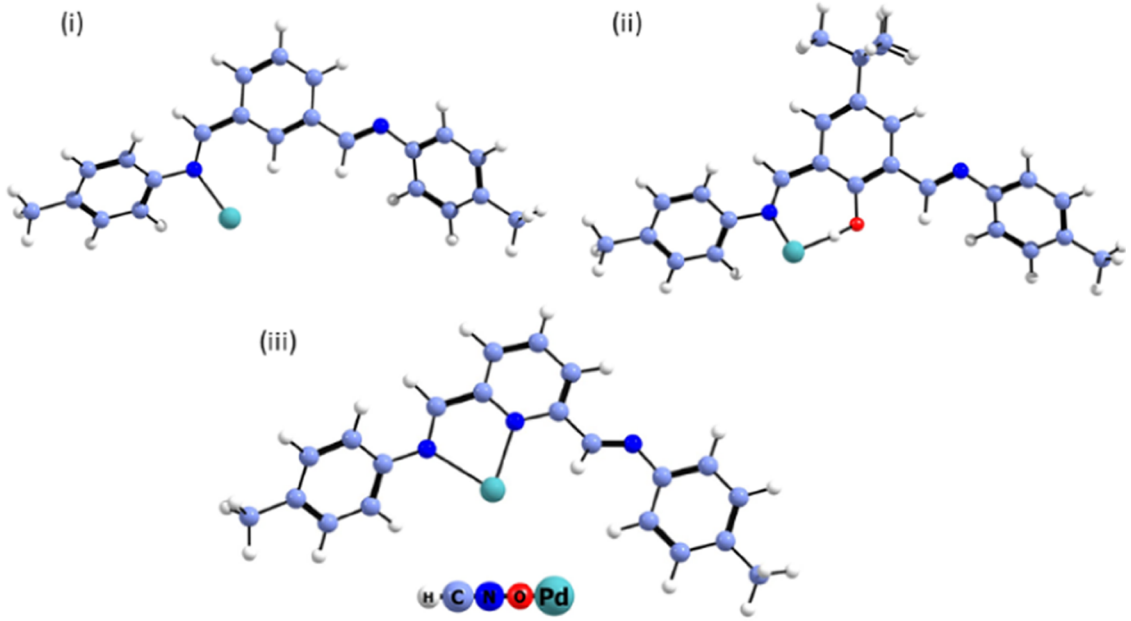

Figure 4. Optimized structures of (i) Pd@TTA−DFB (N), (ii) Pd@TTA−TBD (N∧O), and (iii) Pd@TTA−DFP (N∧N) COFs.

https://doi.org/10.1021/acsami.2c14882
ACS Appl. Mater. Interfaces 2022, 14, 50923−50931

nature, it is important to study the catalytic activity under these circumstances. Similar reaction conditions were adopted from the previously reported Pd/COF-LZU1-catalyzed Suzuki coupling reaction.[33] Bromobenzaldehyde was selected as the reaction substrate, catalyzed by 0.5 mol% of Pd@COFs (Figure 5). Yields >96% were observed in all cases with

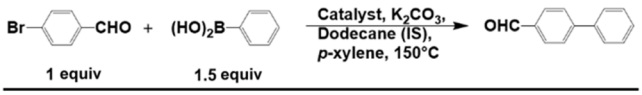

Catalyst	Time (h)	Yield (%)
Pd@TTA-DFB	2	97
Pd@TTA-TBD	4	97
Pd@TTA-DFP	16	96

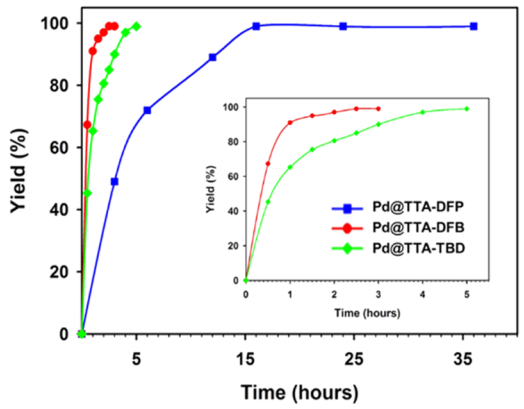

Figure 5. Suzuki−Miyaura cross-coupling of bromobenzaldehyde (1 equiv) with phenyl boronic acid (1.5 equiv) in the presence of 0.5 mol % Pd@COF (catalyst), K_2CO_3 (2 equiv), and *p*-xylene at 150 °C. Yield (%) vs time (hours) plot for the cross-coupling reaction between bromobenzaldehyde and phenyl boronic acid in the presence of Pd@COFs.

complete conversions, showing good catalytic activity in all of the COFs. The kinetics of the reactions are shown in the plots between reaction time vs yield and reaction time vs conversion (Figures 5 and S10). Interestingly, the reaction time required for the complete conversion and yield varied among the three COFs, with Pd@TTA−DFB (N) showing the least time duration (2 h) for completion followed by Pd@TTA−TBD (N∧O) with 4 h. In contrast, a higher conversion time was observed for Pd@TTA−DFP (N∧N), requiring 16 h for completion.

XPS analysis (Figures S6−S8) shows that palladium remains in +2 oxidation state after anchoring onto the COFs. However, for the coupling reaction to occur successfully, Pd(0) is essential. Pd(0) is formed in a preceding step (A) (Scheme S1) before the coupling starts. It has been shown that Pd(0) formation from Pd(II) occurs through the reaction of homocoupling of aryl boronic acids.[44,45] Moreno-Manãs et al. report that the acid-base interactions between palladium and boron groups result in the homocoupling reaction, where Pd(0) is formed as a product of the oxidative homocoupling of aryl boronic acids catalyzed by $Pd(OAc)_2$.[44] To confirm this mechanism for the formation of Pd(0), three homocoupling reactions (with the three Pd@COFs) were performed using only phenyl boronic acid and in the absence of aryl halide to avoid cross-coupling. GC-MS analysis revealed significant formation of biphenyl in all cases, thus confirming Pd(II)-catalyzed homocoupling with the production of Pd(0).[46,47]

We performed reaction kinetics to determine the rate of formation of biphenyl through the homocoupling reaction in the three COFs (Figure S11). A general Suzuki coupling reaction was used with the same parameters as used earlier (except the aryl halide). The amount of biphenyl produced corresponds to the Pd(II) to Pd(0) conversion. This was quantified using GC-MS for the duration of 1 h with intervals of 5 min. It was observed that an equivalent amount of biphenyl is produced corresponding to the palladium loading in the COFs within the first 10 min in all of the cases and the overall quantity remains almost consistent throughout the one hour of the reaction. However, in the case of Pd@TTA−DFP (N∧N), there is no biphenyl formation in the first 5 min, which indicates an induction period. This shows that the overall rate of the reaction for formation of the main product (biphenyl-4-carboxaldehyde) could be affected by the rate of formation of Pd(0) from Pd(II).

To gain more insights into the reactivity of the Pd@COF complexes, the detailed reaction mechanism was investigated using the density functional theory (DFT) at the B3LY-D3(BJ)/6-311++G**/SDD(Pd) level of theory (section S1).[48−54] The proposed mechanism is shown in Figure 6(i). The reaction free energies for the pre-step (1-Pre → 1-biph → 1) for different Pd complexes are first calculated. The observed results suggest that the first step and overall pre-step are favorable for all of the Pd complexes (Figure 6(ii)). However, the last elementary step (1-biph → 1) is endothermic by 7.97 kcal/mol for Pd@TTA−DFP (N∧N) and exothermic by −4.89 and −3.38 kcal/mol for Pd@TTA−TBD (N∧O) and Pd@TTA−DFB (N), respectively. This suggests that the pre-step could be slower in Pd@TTA−DFP (N∧N) compared to that in Pd@TTA−TBD (N∧O) and Pd@TTA−DFB (N). This also corresponds to the experimental observation.

Next, the entire catalytic cycle of the Pd complexes-catalyzed Suzuki−Miyaura cross-coupling reaction was investigated as shown in Figure 6(i). The reaction involves three crucial steps: oxidative addition, transmetalation, and reductive elimination. The reaction starts with the coordination of the R1-Br molecule to **1** for the formation of **2**. The calculated reaction free energies (Figure 6(iii)) were −13.35, −20.22, and −24.82 kcal/mol for Pd@TTA−TBD (N∧O), Pd@TTA−DFB (N), and Pd@TTA−DFP (N∧N), respectively. In the next step, the oxidative addition (**2** → **3**) of the C−Br bond occurs at the Pd center via the transition state (TS1) to form the Pd(II) intermediate (**3**) with energy barriers of 3.71, 4.68, and 7.01 kcal/mol for Pd@TTA−TBD (N∧O), Pd@TTA−DFB (N), and Pd@TTA−DFP (N∧N), respectively (Figure 6). The reaction free energyies (**2** → **3**) changes were calculated to be −28.78, −19.37, and −27.01 kcal/mol for Pd@TTA−TBD (N∧O), Pd@TTA−DFB (N), and Pd@TTA−DFP (N∧N), respectively. The reaction between **3** and K_2CO_3 releases the Br^- anion in the form of KBr and formation of **4** takes place. For this step, the calculated reaction free energies were 4.33, −12.43, and 0.48 kcal/mol for TBD, DFB, and DFP, respectively. After that, the transmetalation (**4** → **5**) process takes place using R_2-$B(OH)_2$ and it was highly exothermic for all of the Pd complexes. The reaction free energies for this step were obtained to be −42.79, −30.62, and −41.92 kcal/mol for Pd@TTA−TBD (N∧O), Pd@TTA−DFB (N), and Pd@TTA−DFP (N∧N), respectively. The reaction completes by the formation of the C−C bond through the reduction

https://doi.org/10.1021/acsami.2c14882
ACS Appl. Mater. Interfaces 2022, 14, 50923−50931

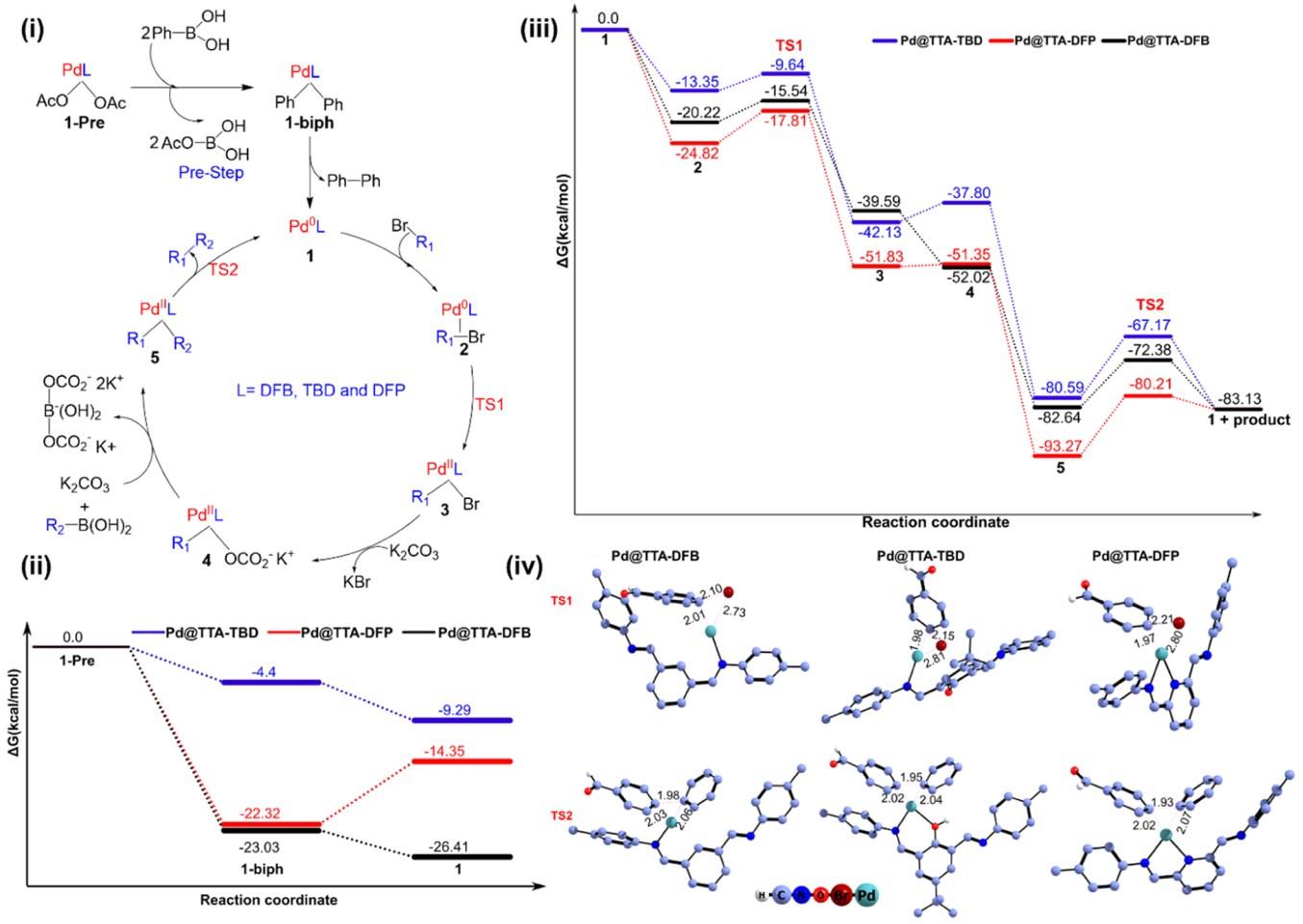

Figure 6. (i) Proposed catalytic cycle for the Suzuki–Miyaura cross-coupling reaction catalyzed by different Pd@COF complexes used to perform the DFT studies; (ii) calculated reaction free energies for the pre-step of Pd@COF complexes at B3LY-D3(BJ)/6–311++G**/SDD(Pd) level of theory; (iii) calculated reaction free energies for the Suzuki–Miyaura cross-coupling reaction catalyzed by Pd@COF complexes; and (iv) optimized transition states (TS1 and TS2) for Pd@TTA–DFB (N), Pd@TTA–TBD (N∧O), and Pd@TTA–DFP (N∧N) COFs. H atoms are omitted for clarity. Bond lengths are in Å.

elimination process (**5** → **1**), where the final product is released from the Pd complexes. The C–C bond formation (**5** → **1**) occurs via the transition state (TS2) with an energy barrier of 13.42, 10.26, and 13.06 kcal/mol for Pd@TTA–TBD (N∧O), Pd@TTA–DFB (N), and Pd@TTA–DFP (N∧N), respectively. On the other hand, the reaction free energy changes for C–C bond formation were −2.54, −0.49, and 10.14 kcal/mol for Pd@TTA–TBD (N∧O), Pd@TTA–DFB (N), and Pd@TTA–DFP (N∧N), respectively.

The theoretical investigation suggests that the Suzuki–Miyaura coupling reaction is thermodynamically favorable for all of the Pd complexes, which agrees well with the overall experimental results. Moreover, all of the elementary steps are exothermic for Pd@TTA–DFB (N) with the highest energy barrier of 10.26 kcal/mol, which is quite reasonable, as in the experiment the reaction completes within 2 h. On the other hand, Pd@TTA–DFP (N∧N) shows the energy barrier of 13.06 kcal/mol for the C–C formation step with the energy change of 10.26 kcal/mol. This infers toward the slow kinetics of Pd@TTA–DFP (N∧N) and supports the experimental observation that the reaction takes 16 h to complete. Pd@TTA–TBD (N∧O) also shows the highest barrier of 13.42 kcal/mol, but all of the elementary steps are thermodynamically favorable except **3** → **4** (4.33 kcal/mol), which makes the reaction kinetics slower than Pd@TTA–DFB (N) and faster than Pd@TTA–DFP (N∧N); hence, the reaction takes four hours for completion. Furthermore, we evaluated the molecular orbitals to find out the primary reason behind the different kinetics of Pd@COFs. For all modelled Pd@COFs, the highest occupied molecular orbital (HOMO) and lowest unoccupied molecular orbital (LUMO) of intermediates **1** and **5** were calculated (Figure 7), as these intermediates show interchangeable oxidation states (0 to +2) during the course of reaction. The HOMO of **1** releases two electrons and becomes LUMO in **5**. During this oxidation process, the energy of HOMO gets destabilized as the position of the newly formed LUMO is lower in energy. On the other hand, during the reduction process **5** gains two electrons to form **1**, and the LUMO of **5** stabilizes into HOMO in **1**. We found that the energy differences between the HOMO of **1** and LUMO of **5** are 1.29, 2.03, and 2.41 eV for Pd@TTA–DFP (N∧N), Pd@TTA–DFB (N), and Pd@TTA–TBD (N∧O), respectively. This suggests that the destabilization energy is the lowest in Pd@TTA–DFP (N∧N), resulting in a more favorable **1** → **5** reaction, whereas during the reductive elimination, Pd@TTA–TBD (N∧O) has the highest stabilization energy, which favors the reaction **5** → **1**. Overall, Pd@TTA–DFP (N∧N) favors the oxidative addition more and Pd@TTA–TBD (N∧O)

https://doi.org/10.1021/acsami.2c14882
ACS Appl. Mater. Interfaces 2022, 14, 50923–50931

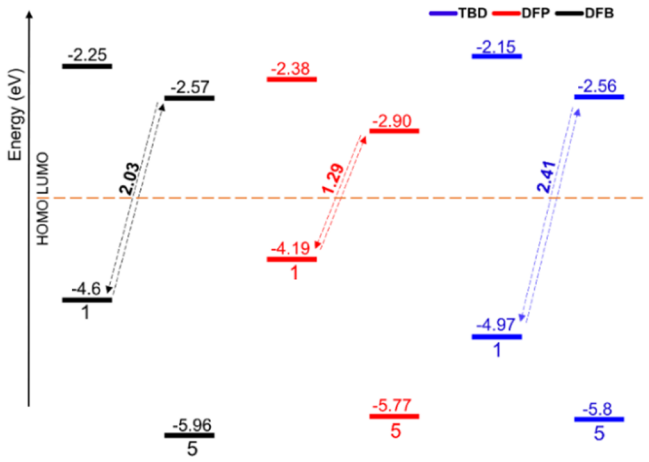

Figure 7. Frontier molecular orbital energy of intermediates **1** and **5** of Pd@COFs at the B3LY-D3(BJ)/6-311++G**/SDD(Pd) level of theory.

favors reductive elimination. On the other hand, Pd@TTA−DFB (N) with the moderate energy difference of 2.03 eV can kinetically balance both oxidation (**1** → **5**) and reduction (**5** → **1**) processes.

The heterogeneity of the catalyst was tested through the hot filtration test, where the reaction is stopped before the completion time and the Pd@COF catalyst is separated from the mixture. The reaction is then allowed to continue without the presence of the active catalyst. In the case of Pd@TTA−DFB (N) COF, leaching was observed, which may be due to the lower number of coordinating sites in the COF. This can also be the reason for the quicker reaction completion time (2 h), as the reaction can occur through the homogeneous route. $Pd(OAc)_2$ was used as a homogeneous catalyst under the same reaction conditions and it was observed that the conversion was 100% within 1 h of the reaction. This further shows that the high activity in Pd@TTA−DFB (N) COF is due to the leached Pd. In the case of Pd@TTA−TBD (N∧O) and Pd@TTA−DFP (N∧N) COFs, the product analysis shows that there is no conversion after filtering the Pd@COFs. XRF and ICP-OES analysis showed 7.1 and 10.5 wt % Pd on the filtered COF powders, and no Pd was detected in the filtrate solution. This further confirms the absence of leaching in these two catalysts. These results show that coordination strength of bidentate ligands (N∧N, N∧O) is stronger than that of the mondentate ligand (N) and thus, a useful design strategy to overcome leaching issues. The turnover frequency (TOF) calculated at 30 min after the reaction for Pd@TTA−DFB, Pd@TTA−TBD, and Pd@TTA−DFP COFs is 1820, 1220, and 220 (h^{-1}), respectively (Table S4). Further, tests of the cross-coupling reactions with a wide substrate scope (Table S3) were performed. In all of the cases >95% yield was observed, proving that Pd@COF can be used for different substrates.

In conclusion, we have synthesized three imine COFs with careful selection of the starting linkers, which provides a base for engineering three crystalline COFs as a support for the active palladium catalyst. A simple strategy is followed, which allows easy formation of ancillary ligands containing N, N∧O, and N∧N active sites. Pd@TTA−DFB (N) shows complete conversion in the shortest time (2 h) in comparison to Pd@TTA−TBD (N∧O) (4 h) and Pd@TTA−DFP (N∧N) (16 h). As a preceding step for the Suzuki coupling reaction, the formation of Pd(0) occurs through the homocoupling reaction of aryl boronic acids. Computational studies reveal the differences between the different reaction kinetics of the COFs. The lower number of coordinating N atoms in Pd@TTA−DFB (N) decreases the metal loading capacity in comparison with the bidentate ligand-containing COFs. This also causes the leaching in Pd@TTA−DFB (N) COFs. The heterogeneity of the Pd@TTA−TBD (N∧O) and Pd@TTA−DFP (N∧N) COFs are confirmed with hot filtration tests combined with XRF and ICP-OES analysis of the filtrates, which show no leaching. The catalyst could also be used up to at least three runs with no significant loss in activity. This study provides an example of linker engineering in COFs and highlights the impact of the coordination nature of $Pd(OAc)_2$ in a heterogeneous catalyst on Suzuki−Miyaura cross-coupling reactions. Such linker engineering allows for simple yet effective COFs, satisfying the strong coordination site requirements, and can be explored further for several important organometallic reactions.[40]

■ ASSOCIATED CONTENT

Supporting Information

The Supporting Information is available free of charge at https://pubs.acs.org/doi/10.1021/acsami.2c14882.

Contains materials and instrumentation details (Section S1); contains the synthesis procedures, elemental analysis, FT-IR spectra, PXRD patterns of the COFs, N2 sorption isotherms, XPS spectra, catalysis results, and substrate scope (Section S2); contains the coordinates of all calculated structures (Section S3) (PDF)

■ AUTHOR INFORMATION

Corresponding Authors

Chidharth Krishnaraj − *COMOC-Center for Ordered Materials, Organometallics and Catalysis, Department of Chemistry, Ghent University, 9000 Ghent, Belgium;* orcid.org/0000-0001-8625-7322; Email: chidharthk@gmail.com

Pascal Van Der Voort − *COMOC-Center for Ordered Materials, Organometallics and Catalysis, Department of Chemistry, Ghent University, 9000 Ghent, Belgium;* orcid.org/0000-0002-1248-479X; Email: pascal.vandervoort@ugent.be

Authors

Himanshu Sekhar Jena − *COMOC-Center for Ordered Materials, Organometallics and Catalysis, Department of Chemistry, Ghent University, 9000 Ghent, Belgium;* orcid.org/0000-0002-5869-5226

Kuber Singh Rawat − *Center for Molecular Modeling (CMM), Ghent University, B-9052 Ghent, Belgium;* orcid.org/0000-0002-7308-4204

Johannes Schmidt − *Department of Chemistry/Functional Materials, Technische Universität Berlin, 10623 Berlin, Germany*

Karen Leus − *COMOC-Center for Ordered Materials, Organometallics and Catalysis, Department of Chemistry, Ghent University, 9000 Ghent, Belgium*

Veronique Van Speybroeck − *Center for Molecular Modeling (CMM), Ghent University, B-9052 Ghent, Belgium;* orcid.org/0000-0003-2206-178X

https://doi.org/10.1021/acsami.2c14882
ACS Appl. Mater. Interfaces 2022, 14, 50923−50931

Complete contact information is available at:
https://pubs.acs.org/10.1021/acsami.2c14882

Author Contributions

[‖]C.K. and H.S.J. contributed equally. The manuscript was written through the contributions of all authors. All authors have given approval to the final version of the manuscript.

Notes

The authors declare no competing financial interest.

■ ACKNOWLEDGMENTS

This work is supported by the Research Board of Ghent University (BOF) through a Concerted Research Action (GOA010-17). The computational resources and services used were provided by Ghent University (Stevin Supercomputer Infrastructure) and the VSC (Flemish Super-computer Center), funded by the Research Foundation-Flanders (FWO).

■ REFERENCES

(1) Geng, K.; He, T.; Liu, R.; Dalapati, S.; Tan, K. T.; Li, Z.; Tao, S.; Gong, Y.; Jiang, Q.; Jiang, D. Covalent Organic Frameworks: Design, Synthesis, and Functions. *Chem. Rev.* **2020**, *120*, 8814−8933.

(2) Bourda, L.; Krishnaraj, C.; Van Der Voort, P.; Van Hecke, K. Conquering The Crystallinity Conundrum: Efforts to Increase Quality of Covalent Organic Frameworks. *Mater. Adv.* **2021**, *2*, 2811−2845.

(3) Mohammed, A. K.; Shetty, D. Macroscopic Covalent Organic Framework Architectures for Water Remediation. *Environ. Sci.: Water Res. Technol.* **2021**, *7*, 1895−1927.

(4) Chen, H.; Liu, W.; Cheng, L.; Meledina, M.; Meledin, A.; Van Deun, R.; Leus, K.; Van Der Voort, P. Amidoxime-Functionalized Covalent Organic Framework as Simultaneous Luminescent Sensor and Adsorbent for Organic Arsenic from Water. *Chem. Eng. J.* **2022**, *429*, No. 132162.

(5) Krishnaraj, C.; Jena, H. S.; Leus, K.; Van Der Voort, P. Covalent Triazine Frameworks − A Sustainable Perspective. *Green Chem.* **2020**, *22*, 1038−1071.

(6) Furukawa, H.; Yaghi, O. M. Storage of Hydrogen, Methane, and Carbon Dioxide in Highly Porous Covalent Organic Frameworks for Clean Energy Applications. *J. Am. Chem. Soc.* **2009**, *131*, 8875−8883.

(7) Keller, N.; Calik, M.; Sharapa, D.; Soni, H. R.; Zehetmaier, P. M.; Rager, S.; Auras, F.; Jakowetz, A. C.; Görling, A.; Clark, T.; Bein, T. Enforcing Extended Porphyrin J-Aggregate Stacking in Covalent Organic Frameworks. *J. Am. Chem. Soc.* **2018**, *140*, 16544−16552.

(8) Sharma, R. K.; Yadav, P.; Yadav, M.; Gupta, R.; Rana, P.; Srivastava, A.; Zbořil, R.; Varma, R. S.; Antonietti, M.; Gawande, M. B. Recent Development of Covalent Organic Frameworks (COFs): Synthesis and Catalytic (Organic-Electro-Photo) Applications. *Mater. Horiz.* **2020**, *7*, 411−454.

(9) Krishnaraj, C.; Jena, H. S.; Bourda, L.; Laemont, A.; Pachfule, P.; Roeser, J.; Vinod Chandran, C.; Borgmans, S.; Rogge, S. M. J.; Leus, K.; Stevens, C. V.; Martens, J. A.; Van Speybroeck, V.; Breynaert, E.; Thomas, A.; Van Der Voort, P. Strongly Reducing (Diarylamino)-Benzene-Based Covalent Organic Framework for Metal-Free Visible Light Photocatalytic H_2O_2 Generation. *J. Am. Chem. Soc.* **2020**, *142*, 20107−20116.

(10) Zhi, Y.; Wang, Z.; Zhang, H.-L.; Zhang, Q. Recent Progress in Metal-Free Covalent Organic Frameworks as Heterogeneous Catalysts. *Small* **2020**, *16*, No. 2001070.

(11) Mullangi, D.; Nandi, S.; Shalini, S.; Sreedhala, S.; Vinod, C. P.; Vaidhyanathan, R. Pd Loaded Amphiphilic COF as catalyst for Multi-Fold Heck Reactions, C-C Couplings and CO Oxidation. *Sci. Rep.* **2015**, *5*, No. 10876.

(12) Chakraborty, D.; Nandi, S.; Mullangi, D.; Haldar, S.; Vinod, C. P.; Vaidhyanathan, R. Cu/Cu_2O Nanoparticles Supported on a Phenol-Pyridyl COF as a Heterogeneous Catalyst for the Synthesis of Unsymmetrical Diynes via Glaser-Hay Coupling. *ACS Appl. Mater. Interfaces* **2019**, *11*, 15670−15679.

(13) Ma, H.-C.; Kan, J.-L.; Chen, G.-J.; Chen, C.-X.; Dong, Y.-B. Pd NPs-Loaded Homochiral Covalent Organic Framework for Heterogeneous Asymmetric Catalysis. *Chem. Mater.* **2017**, *29*, 6518−6524.

(14) Chen, H.; Liu, W.; Laemont, A.; Krishnaraj, C.; Feng, X.; Rohman, F.; Meledina, M.; Zhang, Q.; Van Deun, R.; Leus, K.; Van Der Voort, P. A Visible-Light-Harvesting Covalent Organic Framework Bearing Single Nickel Sites as A Highly Efficient Sulfur-Carbon Cross-Coupling Dual Catalyst. *Angew. Chem.* **2021**, *133*, 10915−10922.

(15) Vardhan, H.; Al-Enizi, A. M.; Nafady, A.; Pan, Y.; Yang, Z.; Gutiérrez, H. R.; Han, X.; Ma, S. Single-Pore Versus Dual-Pore Bipyridine-Based Covalent-Organic Frameworks: An Insight into the Heterogeneous Catalytic Activity for Selective C-H Functionalization. *Small* **2021**, *17*, No. 2003970.

(16) Liu, Y.; Zhou, W.; Teo, W. L.; Wang, K.; Zhang, L.; Zeng, Y.; Zhao, Y. Covalent-Organic Framework-Based Composite Materials. *Chem* **2020**, *6*, 3172−3202.

(17) Gonçalves, R. S. B.; de Oliveira, A. B. V.; Sindra, H. C.; Archanjo, B. S.; Mendoza, M. E.; Carneiro, L. S. A.; Buarque, C. D.; Esteves, P. M. Heterogeneous Catalysis by Covalent Organic Frameworks (COF): $Pd(Oac)_2$@COF-200 in Cross-Coupling Reactions. *ChemCatChem* **2016**, *8*, 743−750.

(18) Shi, Y.; Zhang, X.; Liu, H.; Han, J.; Yang, Z.; Gu, L.; Tang, Z. Metalation of Catechol-Functionalized Defective Covalent Organic Frameworks for Lewis Acid Catalysis. *Small* **2020**, *16*, No. 2001998.

(19) Leng, W.; Peng, Y.; Zhang, J.; Lu, H.; Feng, X.; Ge, R.; Dong, B.; Wang, B.; Hu, X.; Gao, Y. Sophisticated Design of Covalent Organic Frameworks with Controllable Bimetallic Docking For A Cascade Reaction. *Chem. - Eur. J.* **2016**, *22*, 9087−9091.

(20) Chen, R.; Wang, Y.; Ma, Y.; Mal, A.; Gao, X.-Y.; Gao, L.; Qiao, L.; Li, X.-B.; Wu, L.-Z.; Wang, C. Rational Design of Isostructural 2D Porphyrin-Based Covalent Organic Frameworks for Tunable Photocatalytic Hydrogen Evolution. *Nat. Commun.* **2021**, *12*, No. 1354.

(21) Yang, J.; Wu, Y.; Wu, X.; Liu, W.; Wang, Y.; Wang, J. An N-Heterocyclic Carbene-Functionalised Covalent Organic Framework with Atomically Dispersed Palladium for Coupling Reactions Under Mild Conditions. *Green Chem.* **2019**, *21*, 5267−5273.

(22) Gropp, C.; Canossa, S.; Wuttke, S.; Gándara, F.; Li, Q.; Gagliardi, L.; Yaghi, O. M. Standard Practices of Reticular Chemistry. *ACS Cent. Sci.* **2020**, *6*, 1255−1273.

(23) Bagheri, A. R.; Aramesh, N. Towards the Room-Temperature Synthesis of Covalent Organic Frameworks: A Mini-Review. *J. Mater. Sci.* **2021**, *56*, 1116−1132.

(24) Krishnaraj, C.; Kaczmarek, A. M.; Jena, H. S.; Leus, K.; Chaoui, N.; Schmidt, J.; Van Deun, R.; Van Der Voort, P. Triggering White-Light Emission in A 2D Imine Covalent Organic Framework Through Lanthanide Augmentation. *ACS Appl. Mater. Interfaces* **2019**, *11*, 27343−27352.

(25) Miyaura, N.; Suzuki, A. Palladium-Catalyzed Cross-Coupling Reactions of Organoboron Compounds. *Chem. Rev.* **1995**, *95*, 2457−2483.

(26) Koshvandi, A. T. K.; Heravi, M. M.; Momeni, T. Current Applications of Suzuki-Miyaura Coupling Reaction in the Total Synthesis of Natural Products: An Update. *App. Org. Chem.* **2018**, *32*, No. e42.

(27) Mai, S.; Li, W.; Li, X.; Zhao, Y.; Song, Q. Palladium-Catalyzed Suzuki-Miyaura Coupling of Thioureas or Thioamides. *Nat. Commun.* **2019**, *10*, No. 5709.

(28) Barder, T. E.; Walker, S. D.; Martinelli, J. R.; Buchwald, S. L. Catalysts for Suzuki-Miyaura Coupling Processes: Scope and Studies of the Effect of Ligand Structure. *J. Am. Chem. Soc.* **2005**, *127*, 4685−4696.

(29) Meconi, G. M.; Vummaleti, S. V. C.; Luque-Urrutia, J. A.; Belanzoni, P.; Nolan, S. P.; Jacobsen, H.; Cavallo, L.; Solà, M.; Poater, A. Mechanism of the Suzuki-Miyaura Cross-Coupling Reaction Mediated by [Pd(NHC)(Allyl)Cl] Precatalysts. *Organometallics* **2017**, *36*, 2088−2095.

(30) Ahadi, A.; Rostamnia, S.; Panahi, P.; Wilson, L. D.; Kong, Q.; An, Z.; Shoukouhimehr, M. Palladium Comprising Dicationic Bipyridinium Supported Periodic Mesoporous Organosilica (PMO): Pd@Bipy-PMO as an Efficient Hybrid Catalyst for Suzuki-Miyaura Cross-Coupling Reaction in Water. *Catalysts* **2019**, *9*, 140.
(31) Liu, Y.; Wang, J.; Li, T.; Zhao, Z.; Pang, W. Base-Free Pd-MOF Catalyzed the Suzuki-Miyaura Cross-Coupling Reaction of Arenediazonium Tetrafluoroborate Salts with Arylboronic Acids. *Tetrahedron* **2019**, *75*, No. 130540.
(32) Guillén, E.; Rico, R.; López-Romero, M.; Bedia, J.; Rosas, J. M.; Rodríguez-Mirasol, J.; Cordero, T. Pd-Activated Carbon Catalysts for Hydrogenation and Suzuki Reactions. *Appl. Catal. A* **2009**, *368*, 113−120.
(33) Ding, S.-Y.; Gao, J.; Wang, Q.; Zhang, Y.; Song, W.-G.; Su, C.-Y.; Wang, Wei W. Construction of Covalent Organic Framework for Catalysis: Pd/COF-LZU1 in Suzuki-Miyaura Coupling Reaction. *J. Am. Chem. Soc.* **2011**, *133*, 19816−19822.
(34) Romero-Muñiz, I.; Mavrandonakis, A.; Albacete, P.; Vega, A.; Briois, V.; Zamora, F.; Platero-Prats, A. E. Unveiling the Local Structure of Palladium Loaded into Imine-Linked Layered Covalent Organic Frameworks for Cross-Coupling Catalysis. *Angew. Chem., Int. Ed.* **2020**, *59*, 13013−13020.
(35) Li, X.; Van Zeeland, R.; Maligal-Ganesh, R. V.; Pei, Y.; Power, G.; Stanley, L.; Huang, W. Impact of Linker Engineering on the Catalytic Activity of Metal-Organic Frameworks Containing Pd(II)-Bipyridine Complexes. *ACS Catal.* **2016**, *6*, 6324−6328.
(36) Yan, S.; Guan, X.; Li, H.; Li, D.; Xue, M.; Yan, Y.; Valtchev; Qiu, S.; Fang, Q. Three-Dimensional Salphen-Based Covalent-Organic Frameworks as Catalytic Antioxidants. *J. Am. Chem. Soc.* **2019**, *141*, 2920−2924.
(37) Guo, X.; Li, Y.; Zhang, M.; Cao, K.; Tian, Y.; Qi, Y.; Li, S.; Li, K.; Yu, X.; Ma, L. Colyliform Crystalline 2D Covalent Organic Frameworks (COFs) with Quasi-3D Topologies for Rapid I2 Adsorption. *Angew. Chem., Int. Ed.* **2020**, *59*, 22697−22705.
(38) Yusran, Y.; Li, H.; Guan, X.; Li, D.; Tang, L.; Xue, M.; Zhuagn, Z.; Yan, Y.; Valtchev, V.; Qiu, S.; Fang, Q. Exfoliated Mesoporous 2D Covalent Organic Frameworks for High-Rate Electrochemical Double-Layer Capacitors. *Adv. Mater.* **2020**, *32*, No. 1907289.
(39) Wang, C.; Zhang, Z.; Zhu, Y.; Yang, C.; Wu, J.; Hu, W. 2D Covalent Organic Frameworks: From Synthetic Strategies to Advanced Optical-Electrical-Magnetic Functionalities. *Adv. Mater.* **2022**, *34*, No. 2102290.
(40) Zhang, N.; Wang, T.; Wu, X.; Jiang, C.; Chen, F.; Bai, W.; Bai, R. Self-exfoliation of 2D Covalent Organic Frameworks: Morphology Transformation Induced by Solvent Polarity. *RSC Adv.* **2018**, *8*, 3803−3808.
(41) Haldar, S.; Roy, K.; Kushwaha, R.; Ogale, S.; Vaidhyanathan, R. Chemical Exfoliation as a Controlled Route to Enhance the Anodic Performance of COF in LIB. *Adv. Energy Mater.* **2019**, *9*, No. 1902428.
(42) Fache, F.; Schulz, E.; Tommasino, M. L.; Lemaire, M. Nitrogen-Containing Ligands for Asymmetric Homogeneous and Heterogeneous Catalysis. *Chem. Rev.* **2000**, *100*, 2159−2232.
(43) Tan, H.-Z.; Wang, Z.-Q.; Xu, Z.-N.; Sun, J.; Chen, Z.-N.; Chen, Q.-S.; Chen, Y.; Guo, G.-C. Active Pd(II) Complexes: Enhancing Catalytic Activity by Ligand Effect for Carbonylation of Methyl Nitrite to Dimethyl Carbonate. *Catal. Sci. Technol.* **2017**, *7*, 3785−3790.
(44) Moreno-Mañas, M.; Pérez, M.; Pleixats. Palladium-Catalyzed Suzuki-Type Self-Coupling of Arylboronic Acids. A Mechanistic Study. *J. Org. Chem.* **1996**, *61*, 2346−2351.
(45) Johansson Seechurn, C. C. C.; Sperger, T.; Scrase, T. G.; Schoenebeck, F.; Colacot, T. J. Understanding the Unusual Reduction Mechanism of Pd(II) to Pd(I): Uncovering Hidden Species and Implications in Catalytic Cross-Coupling Reactions. *J. Am. Chem. Soc.* **2017**, *139*, 5194−5200.
(46) Adamo, C.; Amatore, C.; Ciofini, I.; Jutand, A.; Lakmini, H. Mechanism of the Palladium-Catalyzed Homocoupling of Arylboronic Acids: Key Involvement of A Palladium Peroxo Complex. *J. Am. Chem. Soc.* **2006**, *128*, 6829−6836.
(47) Gupta, K. C.; Sutar, A. K. Catalytic Activities of Schiff Base Transition Metal Complexes. Coord. *Coord. Chem. Rev.* **2008**, *252*, 1420−1450.
(48) Becke, A. D. Density-Functional Exchange-Energy Approximation with Correct Asymptotic Behavior. *Phys. Rev. A.* **1988**, *38*, 3098.
(49) Lee, C.; Yang, W.; Parr, R. G. Development of the Colle-Salvetti Correlation-Energy Formula into A Functional of the Electron Density. *Phys. Rev. B.* **1988**, *37*, 785.
(50) Fuentealba, P.; Stoll, H.; Szentpaly, Lv.; Schwerdtfeger, P.; Preuss, H. On the Reliability of Semi-Empirical Pseudopotentials: Simulation of Hartree-Fock and Dirac Results. *J. Phys. B: At. Mol. Phys.* **1983**, *16*, L323.
(51) Andrae, D.; Haussermann, U.; Dolg, M.; Stoll, H.; Preuss, H. Energy-Adjusted Ab Initio Pseudopotentials for the Second and Third Row Transition Elements. *Theor. Chim. Acta.* **1990**, *77*, 123−141.
(52) Hariharan, P. C.; Pople, J. A. The Influence of Polarization Functions on Molecular Orbital Hydrogenation Energies. *Theor. Chim. Acta* **1973**, *28*, 213−222.
(53) Francl, M. M.; Pietro, W. J.; Hehre, W. J.; Binkley, J. S.; Gordon, M. S.; DeFrees, D. J.; Pople, J. A. Self-Consistent Molecular Orbital Methods. XXIII. A Polarization-Type Basis Set for Second-Row Elements. *J. Chem. Phy.* **1982**, *77*, 3654−3665.
(54) Grimme, S.; Ehrlich, S.; Goerigk, L. Effect of the Damping Function in Dispersion Corrected Density Functional Theory. *J. Comput. Chem.* **2011**, *32*, 1456−1465.

https://doi.org/10.1021/acsami.2c14882
ACS Appl. Mater. Interfaces 2022, 14, 50923−50931